

Orientalional Ordering, Locking-in, and Distortion of CH₄ Molecules in Methane Hydrate III under High Pressure

Sofiane Schaack,[†] Umberto Luca Ranieri,^{‡,§} Philippe Depondt,[†] Richard Gaal,[§] Werner F. Kuhs,^{||} Andrzej Falenty,^{||} Philippe Gillet,[§] Fabio Finocchi,^{*,†} and Livia E. Bove^{*,§,⊥}

[†]Sorbonne Université, CNRS UMR 7588, Institut des Nanosciences de Paris (INSP), 75005 Paris, France

[‡]Institut Laue-Langevin, 71, avenue des Martyrs, CS 20156, 38042 Grenoble Cedex 9, France

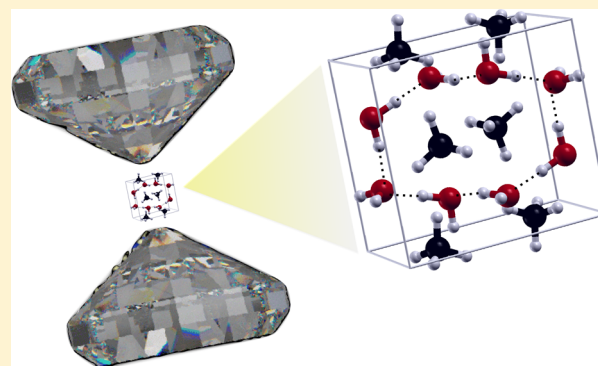
[§]EPFL, ICMP, École polytechnique fédérale de Lausanne (EPFL), Station 3, CH-1015 Lausanne, Switzerland

^{||}GZG Abt. Kristallographie, Universität Göttingen, Goldschmidtstrasse 1, 37077 Göttingen, Germany

[⊥]Sorbonne Université, CNRS UMR 7590, Institut de minéralogie, de physique des matériaux et de cosmochimie (IMPMC), 75005 Paris, France

Supporting Information

ABSTRACT: We investigate the effects of high pressure on the reorientational and vibrational dynamics of methane molecules embedded in methane hydrate III—the stable form of methane for pressures above 2 GPa at room temperature—by combining high-pressure Raman spectroscopy with ab initio simulations including nuclear quantum effects. We observe a clear evolution of the system from a gas-filled ice structure, where methane molecules occupy the channels of the ice skeleton and rotate almost freely, to a CH₄:D₂O compound where methane rotations are hindered, and methane and water dynamics are tightly coupled. The gradual orientational ordering of the guest molecules results in a complete locking-in at approximately 20 GPa. This happens along with a progressive distortion of the guest molecules. Finally, as pressure increases beyond 20 GPa, the system enters a strong mode coupling regime where methane guests and water hosts dynamics are intimately paired.



INTRODUCTION

Ice clathrates are inclusion compounds wherein small nonpolar gas (guest) molecules are enclosed inside polyhedral cavities, or cages, formed by hydrogen-bonded water (host) molecules.^{1,2} The interaction between the guest molecule and the ice skeleton is mostly repulsive, which makes clathrate hydrates interesting prototypes for the study of hydrophobic interactions that are encountered in the more complex living matter.³ Clathrate hydrates can be stabilized by rather modest pressure, typically in the megapascal range, depending on the specific guest gas molecule, and once formed they keep the guest molecules efficiently trapped at low temperature. For this reason, they are envisaged as potentially attractive hosting environments for physical hydrogen storage^{4,5} or for CO₂ sequestrations.⁶ Among the different clathrate hydrates, methane hydrate is the most widespread naturally occurring gas hydrate as it is present in large quantities in subsurface deposits, both in oceanic shelf sediments and in permafrost regions.⁷ Methane hydrates are also suspected to exist at depth in many water-rich objects populating the outer solar system.⁸ Therefore, several experimental studies in the last years focused on the high-pressure behavior of methane hydrates.^{8–24}

As pressure increases beyond the kilobar range, typically above 1–2 GPa, most ice clathrates undergo profound structural changes: the cages shrink and reorganize into structures bearing some resemblance to ice phases, known as filled ices,⁹ where the guest molecules occupy interstices in the ice lattices.¹⁰ In filled ices, three different structures have been observed so far, and more recently, a new “chiral hydrate” was established.^{25,26}

Many entangled phenomena are expected to occur in the system as pressure rises, such as the change in nature of the guest–host interaction, the likely coupling of guest and host dynamics, and possibly orientational ordering of the guests and structure rearrangements. At moderate pressures, a coupling between the localized rattling modes of the guests and the host lattice phonons has been recognized as an essential ingredient for stabilizing the clathrate structure.^{27,28} As the pressure rises, the guest molecules are expected to deviate strongly from free rotors because of the increasing interaction with the water frame toward a frozen crystalline structure at very high

Received: March 22, 2018

Revised: April 26, 2018

Published: April 26, 2018

pressure. However, the evolution of the hydrate between these two regimes is rarely investigated. A microscopic description of the behavior of the gas molecules enclosed under tight confinement within the water frame is still lacking, and the nature of the guest–host interaction in this regime remains elusive.

In this paper, we focus on the methane hydrate III (MH-III) phase, which is the stable phase of methane hydrates above 2 GPa at room temperature and shares its filled ice structure with krypton, argon, and nitrogen hydrates.^{8,10} The structure of MH-III is related to ice Ih, especially in the *a*–*b* plane, where it shows characteristic tilted sixfold water rings. The channel-like voids along the *c* axis are filled with methane molecules, with their centers arranged in a zig-zag fashion along the *c* axis. At variance with ice Ih, MH-III has also four- and eightfold water rings. The coexistence of distinct ice rings within the same structure gives MH-III a marked crystalline anisotropy, which is particularly evident at high pressures (see [Supporting Information](#) Figure S7).

High-pressure methane hydrate has been widely investigated by different techniques, including Raman spectroscopy,^{16–21,29} X-ray diffraction,^{9,11–16,21} and neutron diffraction.^{8,9,30} The preparation of hydrates with 90–95% of the maximum theoretical occupation of the guest sites is quite challenging, and the risk of structural destabilization under compression increases drastically if the filling ratio of the starting clathrate is not high enough. MH-III was found to be stable up to 86 GPa at least,¹⁵ though a possible transition to an unresolved high-pressure structure was reported to occur at around 40 GPa.^{14,15,19,21} A splitting of the symmetric (ν_1) and antisymmetric (ν_3) CH stretching mode peaks above 15–20 GPa has also been observed, which some authors attributed to the CH₄ orientational ordering^{14,19,21} and others ascribed to the distortion of the methane molecules at high pressure.²² Finally, the appearance of a possible Fermi resonance between the overtone of the D₂O bending mode and the OD stretching mode was observed²² at 15 GPa, while symmetrization of the hydrogen bond network was predicted to occur above 60 GPa from ab initio molecular simulations.^{22,23} However, a clear interpretation of the previous observations and a unified picture of the interplay of those different phenomena are still lacking.

In the following, we investigate the pressure effects on the reorientational and vibrational motion of the methane molecules embedded in MH-III, as well as the modification of the host–guest coupling, by combining high-resolution Raman spectroscopy under high pressure with ab initio density functional theory molecular dynamics (DFT-MD) simulations,³¹ including nuclear quantum effects through the quantum thermal bath (QTB)^{32–35} and path integral-generalized Langevin equation (PI + GLE)³⁶ methods at the 2/1 theoretical ratio of water/methane. Through the analysis of MD trajectories, we anticipate that two pressure domains can be identified: for *P* < 20 GPa, the methane molecules become orientationally ordered as the pressure increases, whereas the guest molecules undergo angular distortions; beyond a pressure threshold of about 20 GPa, methane and water vibrational modes are strongly coupled.

METHODS

Sample Preparation. Starting sI methane clathrate hydrate samples of this study were prepared using a finely ground D₂O ice impregnated with methane gas at 60 bar, following the method described in ref 37. Synthesized samples were kept at

liquid nitrogen temperature and extensively characterized by X-ray and neutron diffraction. The diamond anvil cells (DACs) were cooled to liquid nitrogen temperature and loaded cold with sI methane clathrate hydrate under nitrogen atmosphere in a portable glovebox, to avoid contamination by atmospheric water. A small ruby ball was also trapped to serve as a pressure gauge. Pressure was applied on the cold sample to achieve high enough pressure to stabilize the sample even at room temperature. After the initial pressurization, the samples were warmed up and all measurements were carried out at 300 K. Pressure was varied between 10 and 45 GPa. The absence of hysteresis effects was verified by sweeping the pressure up and down. Compression/decompression rates were typically 2 GPa/h. The starting sI CH₄:D₂O clathrate hydrate sample was also characterized by infrared and Raman scattering and shown to have a 86% methane filling ratio in the small cages and 99% in the big cages. Under slow compression (2 GPa/h ca.), the clathrate transformed with loss of water to the hexagonal clathrate sH at ~1 GPa and then to the MH-III structure at around 2 GPa with further loss of water. Finally, we investigated the pressure dependence of the CH stretching mode and of the CH₄ rocking mode between 3 and 22 GPa during a dedicated Raman experiment. No ruby was used during this loading; pressure was evaluated with a precision of 0.5 GPa based on the measured shift of the diamond Raman signal measured in the center of the culet, compared to earlier runs when both diamond Raman and ruby fluorescence were measured.

High-Pressure Raman Scattering. The pressure dependence of the Raman spectra of CH₄:D₂O was measured with a HR-800 spectrometer using a Cobolt Samba 532 nm laser for excitation and a 600 L/mm grating. The spectrometer is coupled to a microscope, and a Mitutoyo SL50X objective allowed direct measurements inside the DAC. The resolution of the instrument under these conditions is about 0.5 cm⁻¹, as determined from measuring the emission lines of a He–Ne gas lamp. Pressure was generated in a symmetric Mao-type DAC using 300 micron culet type IIs diamonds for minimal fluorescence and monitored by ruby fluorescence using the pressure scale from refs 38 and 39. As the sample signal overlaps with the second-order Raman signal of the diamond, we systematically measured the Raman spectra on the gasket close to the sample chamber and used it as a background, together with a quadratic function to approximate fluorescence from the lower diamond, invisible in the gasket measurements. Details of the procedure are given in the [Supporting Information](#) of our earlier paper.⁴⁰

Simulations. MD simulations at room temperature of both CH₄:(D₂O)₂ and CH₄:(H₂O)₂ methane hydrates were carried out using the QTB method^{32,35} (details in [Supporting Information](#)) and the PI + GLE method,³⁶ to include nuclear quantum effects that are especially important on light nuclei such as H and D. Although a semi-classical approximation, the QTB is quite efficient in computing vibrational spectra,^{35,41} while PI + GLE yields exact distributions in the limit of an infinite number of beads. The samples for the QTB simulations consist of 16 methane molecules and 32 water molecules in a 2 × 1 × 2 orthorhombic supercell, with an initial MH-III structure taken from ref 10. A sample of four methane molecules and eight water molecules with eight beads was used for the PI + GLE simulations. Oxygen and carbon atoms were initially set at their crystallographic positions, while hydrogen (deuterium) atoms were let to relax during short simulations

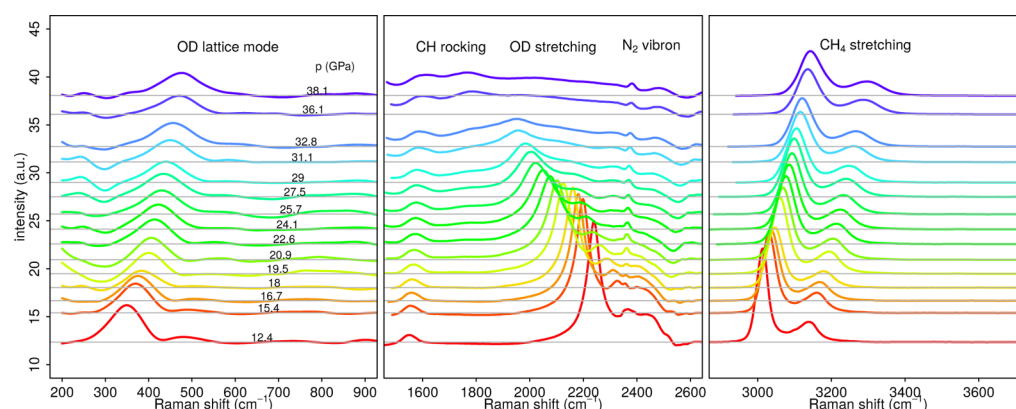


Figure 1. Experimental Raman spectra of the sample at pressures between 12 and 45 GPa. Left: lattice mode; center: CH₄ rocking and OD stretching modes; right: CH stretching modes.

with large friction coefficients γ to explore different configurations and start with variable orientations for the CH₄ molecules. The electronic structure and atomic forces were described within the generalized gradient approximation (GGA)⁴² to the DFT. van der Waals (vdW) interactions were added by following the semi-empirical D2 scheme by Grimme;⁴³ after extensive tests, a better agreement with experimental lattice constants and compressibility could be obtained within GGA + D2 than in the GGA; vibrational spectra are not affected by the introduction of the vdW correction. All calculations were carried out by using the Quantum ESPRESSO package³¹ in combination with a QTB implementation³⁵ or the i-PI package⁴⁴ for PI + GLE. Ultrasoft pseudopotentials were used to describe the interaction between the ionic cores and the valence electrons: a plane-wave expansion cutoff of $E_{\text{cut}} = 40$ Ry ensured convergence of total energy, pressure, and atomic forces. A $2 \times 1 \times 2$ k -point grid sampling was used. Simulations were run at constant volume, with lattice parameters chosen to obtain isotropic stress tensors within the statistical error, in the range 3–45 GPa. The typical duration time of the simulations was 30 ps. The reader can refer to the Supporting Information for technical details.

RESULTS AND DISCUSSION

Pressure Dependence of the Raman Spectra. Raman spectra of a CH₄:D₂O clathrate were measured at room temperature, while the stability of the MH-III structure up to 45 GPa was checked by X-ray diffraction (Supporting Information Figure S1).

In Figure 1, we show the pressure dependence of the background-subtracted Raman spectra over three significant frequency ranges (the full measured spectrum before background subtraction is reported in Supporting Information Figure S2). Several bands related to MH-III disperse with pressure, which we identify as follows: the lattice vibration of the water frame (350–450 cm⁻¹), the rocking of the CH₄ molecules (1550–1600 cm⁻¹), the OD stretching mode of the water frame (1600 and 2400 cm⁻¹), and the symmetric and antisymmetric CH stretching modes (3000 and 3300 cm⁻¹). As the sample contained excess ice, we checked how the OD lattice and stretching modes are measured on the sample compared to those of pure ice (Supporting Information Figure S3).

Figure 2 shows the experimental Raman shifts as the pressure is increased along with the vibrational frequencies provided by

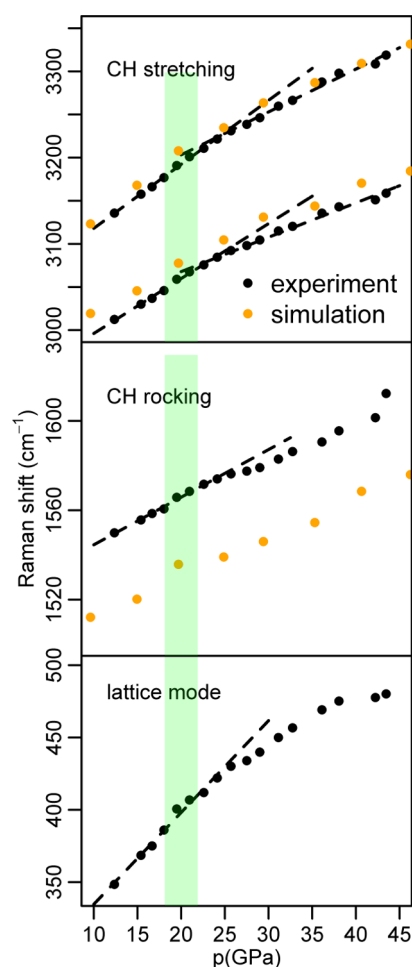


Figure 2. Lattice mode, CH₄ stretching mode frequencies as a function of pressure. Dashed lines are linear fit of the experimental data points below 25 GPa. A deviation from the linear trend is evident for all data points above 25 GPa.

our QTB-MD simulations, for the methane stretching and rocking modes and the D₂O lattice mode. Despite the discrepancy of about 35 cm⁻¹ between the observed and calculated CH₄ rocking mode, the methane rocking mode frequency at 25 GPa is located at a value that is quite similar to the calculated one reported in ref 22 and remains within expected DFT precision. One can notice that an extrapolation from our values to ambient pressure gives values, which are

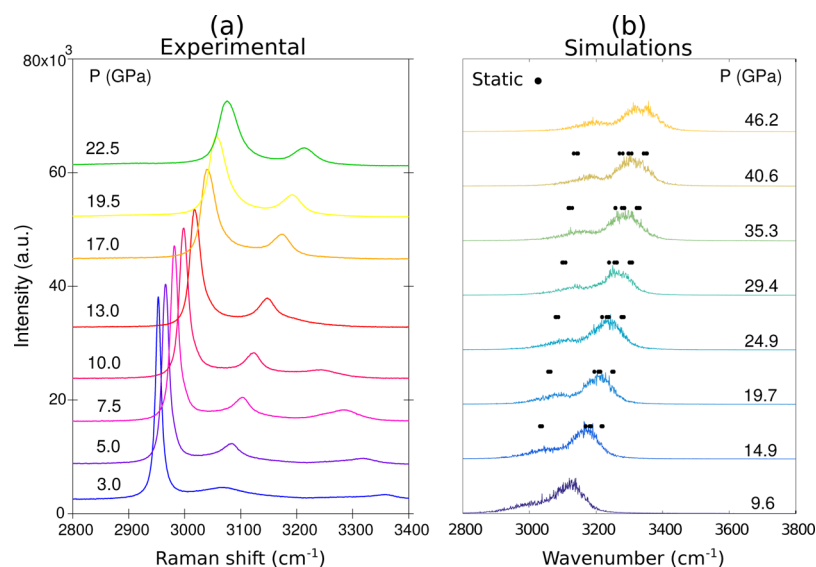


Figure 3. (a) Experimental high-resolution Raman spectra of the CH stretching mode of the sample at different pressures. There was no indication of splitting of peaks as claimed to be observed at approximately 15 GPa in refs.^{14,19,21} (b) Spectra computed from the velocity correlation functions from the simulation trajectories (color lines) and relevant eigenfrequencies from a dynamical matrix analysis (dots).

reasonably close to the calculated rocking mode frequency ($\sim 1450\text{--}1465\text{ cm}^{-1}$) in ref 45. The high quality of the collected Raman data in the full pressure range allows to keep the error bars on the Raman shift smaller than the plotted dots. Details of the fitting procedure are reported in the [Supporting Information](#). The absence of new peaks in our Raman spectra indicates that methane hydrate neither destabilized nor underwent main structural rearrangements, as also observed by X-ray diffraction ([Supporting Information](#) Figure S1). More importantly, our results reveal that the observed vibrational modes follow the same evolution upon compression; in particular, all frequency dependencies on pressure deviate from a simple linear behavior at $P \approx 20\text{ GPa}$. This behavior concerns the modes of both the CH_4 molecules and the D_2O network. The observed changes in the slope of the pressure dependence in both water frame and guest modes around 20 GPa consistently indicate an enhanced coupling of the guest and host dynamics, which has been conjectured but never detailed so far. The calculated spectra quantitatively reproduce all the main features and the trends that we observed in the measured ones.

In particular, the symmetric (ν_1) and antisymmetric (ν_3) CH stretching modes of the methane molecules in MH-III have often been discussed: three works^{14,19,21} reported a splitting correlated with the appearance of a new MH-III phase with orientationally ordered methane molecules. Other authors interpreted that the splitting is due to a CH_4 molecule distortion and to the consequent lift of degeneracy of the methane stretching mode as observed by infrared vibrational spectroscopy.²² The onset of this splitting and its nature are controversial, as it could also be due to a partial destabilization of the MH-III structure under compression and to the consequent appearance of solid methane or of a new hydrate phase promoted by the laser heating.

While our low-pressure data are in excellent agreement with previous authors,^{14,19,21} we observed a different behavior above 15–20 GPa. Specifically, both peaks progressively broaden with pressure (see [Figure 1](#), right panel); however, we detected no splitting of either the ν_1 or ν_3 modes in the range 15–20 GPa

or beyond; details of this frequency range are plotted in [Figure 3](#) and compared with our simulation data. Indeed, the methane stretching mode frequencies as a function of pressure both within the harmonic approximation at $T = 0\text{ K}$ and from our MD trajectories at ambient temperature were computed. The methane stretching mode frequencies computed on the optimized configurations ([Figure 3b](#)) present a lift of degeneracy around 15 GPa for the asymmetric ν_3 mode and around 25 GPa for the symmetric ν_1 mode. However, when at ambient temperature, the dynamics of the molecules is properly taken into account, and the clear-cut splitting (approximately 80 cm^{-1} in the above-mentioned references) rather broadens (approximately 60 cm^{-1}). Within the pressure range of our simulations, we found no evidence of the CH bond length asymmetry beyond the statistical noise.

As far as the data of refs^{14,19,21} are concerned, the additional stretching band indeed matches the frequency of the CH stretching mode in pure methane.^{46,47} We could imagine that in the experiments of refs,^{14,19,21} a partial decomposition of the MH-III structure could have been caused by a low amount of methane in the sample and/or a too fast compression. It has been shown that under fast compression, methane clathrate hydrate transforms into ice VII and solid methane at 2.3 GPa, whereas under slow compression, it transforms into MH-III.^{10–12}

Orientational Ordering. The rotation of the enclosed molecules has often been discussed in filled ices. For comparison, the CH_4 molecules enclosed in metal–organic framework (MOF)⁴⁸ undergo rotational motion; however, methane–methane and methane frame distances are larger than those in MH-III examined here.

Thus, to understand the transition for the methane rotational motion from relatively free to tightly locked to the cage, we studied the orientation, distortion, and vibrational mode coupling of CH_4 in deuterated MH-III (specifically $\text{CH}_4\text{:}(\text{D}_2\text{O})_2$), at room temperature and for pressures between 3 and 45 GPa by MD simulation. Technical details are available in the [Supporting Information](#).

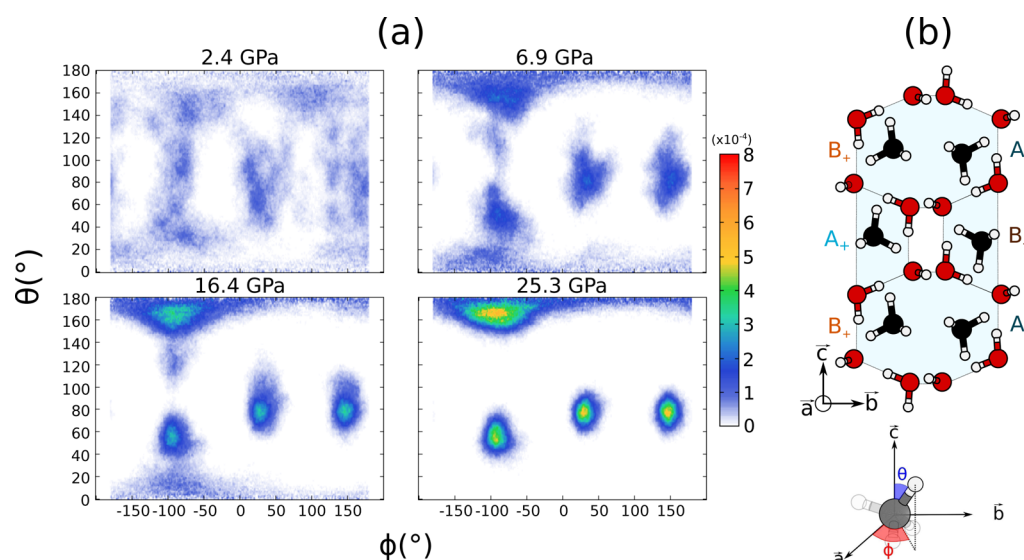


Figure 4. (a) Probability distributions of CH vector polar angles $P_{\text{CH}}(\theta, \phi)$ computed at 6.9, 16.4, 25.3, and 36.4 GPa via PI + GLE for a molecule in a B_{-} configuration. (b) Sketch of the most probable methane configurations A_{\pm} and B_{\pm} .

The orientation of the methane molecules enclosed within the water frame was investigated by calculating the orientational probability density function (OPDF) $P_{\text{CH}}(\theta, \phi)$ of the CH bonds for different pressures: the OPDF for one molecule is shown in Figure 4a. For the sake of simplicity, the high-pressure case ($P = 25.3$ GPa) is considered first: four well-defined peaks corresponding to the four CH bonds are observed. This is a clear indication of an ordered situation. The guests are distributed among the four configurations A_{\pm} and B_{\pm} in the conventions of Figure 4b. The example in Figure 4a described above corresponds to a B_{-} configuration. Thus, the high-pressure structure, schematically represented in Figure 4b, yields A_{+}/B_{-} (or A_{-}/B_{-}) stacking along the b axis, while we observe A_{+}/B_{+} (or A_{-}/B_{-}) stacking along c axis and finally A_{+}/A_{-} (or B_{+}/B_{-}) stacking along a . This picture is not altered as the pressure is increased up to 35 GPa.

In contrast, at low pressure, the picture is rapidly blurred as orientational disorder sets in: new, rather broad, peaks appear while the two peaks at $\phi = 30$ and 150° broaden toward $\theta = 90^{\circ}$. At the two intermediate pressures, namely, 6.9 and 16.4 GPa, the distribution dependence on the angle ϕ remains essentially unaltered, while the θ dependence broadens significantly. We interpret this as a dynamical disorder between A_{+} and A_{-} (and also between B_{+} and B_{-}). Moreover, at the lowest pressure ($P = 2.4$ GPa), one also observes the onset of A/B dynamical disorder.

To summarize, as the pressure is increased from ~ 3 to 45 GPa, $P_{\text{CH}}(\theta, \phi)$ clearly exhibits an increasing anisotropy, which illustrates that the guest methane molecules undergo a definite pressure-induced orientational locking-in in two main steps: first, around 5 GPa, A/B motions disappear, and at approximately 20 GPa, $+/-$ orientations lock-in. In close analogy with pure methane,⁴⁷ it has been conjectured^{19,22} that methane orientational ordering in MH-III could occur at 20 GPa. We provide direct evidence for such an orientational ordering, which turns out not to be absolutely straightforward.

Methane Distortion. The evolution of the six $\widehat{\text{HCH}}$ (α_n , $n = 1, \dots, 6$) angles per methane molecule follows an interesting trend. At low pressure (3 GPa), all angle probability distributions $P(\alpha_n)$ are centered around the tetrahedral angle

of 109.47° . Upon increasing the pressure, two of them shift progressively away from the tetrahedral angle (Figure 5). The agreement between static relaxation and PI + GLE simulations indicates that the dynamics, whether classical or quantum, plays a small role in this issue.

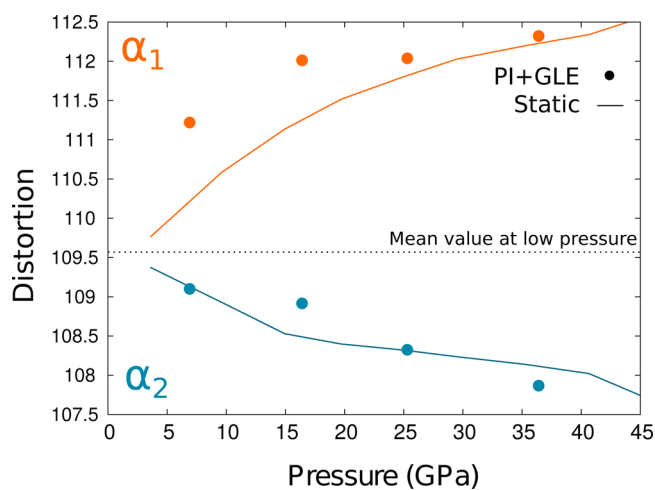


Figure 5. Mean angles $\langle \alpha_{1,2} \rangle$ in CH_4 as a function of pressure from static relaxed configurations and PI + GLE simulations.

We label α_1 the $\widehat{\text{HCH}}$ angles that are close to parallel to the (a,b) plane and α_2 those angles that are in the (b,c) plane. Figure 5 shows that α_1 increases as the pressure is increased, where α_2 decreases from the ideal value, thus making the $\text{H}-\text{H}$ distance decrease along c . The latter effect is due to compression along the c axis, for which the lattice constant decreases rapidly (Supporting Information Figure S7). The former can be understood as the flattening out of the molecule as the nearest neighbors are the hydrogen atoms of the next methane molecule in the b direction.

Mode Mixing. The mode analysis within the harmonic approximation shows that at low pressure ($P < 10$ GPa), the eigenvectors of the CH_4 rocking modes are fully localized on the methane molecules. In contrast, as the pressure increases,

they progressively mix with the atomic displacements of the water frame. To quantify the coupling between the water and the methane molecules, we projected the mode eigenvectors $\vec{e}^{(\nu)}$ at each pressure on atomic displacements that are centered either on the deuterated water frame or on the methane molecules

$$\vec{e}^{(\nu)} = \sum_{i \in \text{D}_2\text{O}} b_i^{(\nu)} \vec{x}_i + \sum_{j \in \text{CH}_4} c_j^{(\nu)} \vec{x}_j \quad (1)$$

where $b_i^{(\nu)}$ and $c_j^{(\nu)}$ are the coefficients of the respective expansions for the mode at frequency ν .

We then calculate a methane participation ratio $P_{\text{CH}_4}(\nu)$ which describes the participation of the methane degrees of freedom (DoF) to the vibrational mode ν .

$$P_{\text{CH}_4}(\nu) = \sum_{\text{CH}_4}^{\text{DoF}} \frac{c_j^{(\nu)^2}}{\vec{e}^{(\nu)} \cdot \vec{e}^{(\nu)}} \quad (2)$$

where the sum runs over all the CH_4 DoF. The same expression holds for $P_{\text{D}_2\text{O}}(\nu)$ in which $c_j^{(\nu)}$ is replaced with $b_i^{(\nu)}$, which ensures that

$$P_{\text{CH}_4}(\nu) + P_{\text{D}_2\text{O}}(\nu) = 1 \quad (3)$$

In the case $P_{\text{CH}_4}(\nu) = 1$, the mode ν is totally characterized by the methane DoF contribution, while if $P_{\text{CH}_4}(\nu) = 0$, it is characterized by the water frame DoF only. Figure 6 shows the

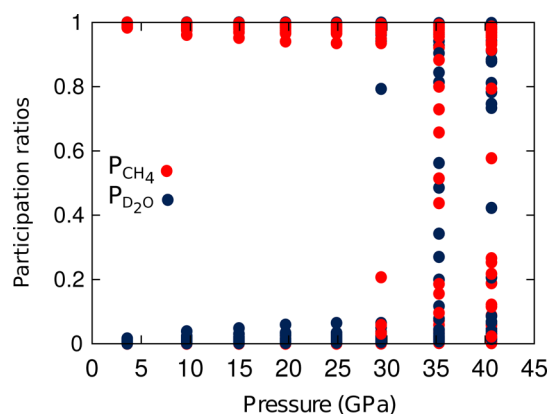


Figure 6. Mode participation ratios for methane (blue) and D_2O frame (red), computed according to eqs 1 and 2.

participation ratios ($P_{\text{CH}_4}, P_{\text{D}_2\text{O}}$) calculated for each methane bending and OD stretching modes as the pressure increases. Up to 20 GPa, $P_{\text{CH}_4} \approx 1$ or 0, the investigated modes are totally described either by the methane or by the water DoF contribution. Starting at 20 GPa, some vibrational modes are described by a combination of the methane and water DoF contributions, leading to a contribution coefficient $0 < P_{\text{CH}_4} < 1$. This behavior describes the pressure-induced mode coupling occurring in MH-III at 20 GPa as it is not possible to attribute these modes to a methane bending or an OD stretching vibrational mode but rather to a mixed one. Their characters therefore deeply change in this pressure range, which could be at the root of the chaotic behavior of the measured OD stretching modes (detailed in Supporting Information Figure S3). We note in passing that the resonance between the CH_4 rocking modes and the water OD stretching modes only occurs

in the deuterated system $\text{CH}_4:\text{D}_2\text{O}$. In the protonated system ($\text{CH}_4:\text{H}_2\text{O}$), another type of resonance takes place between the host and guest vibrational modes. Indeed, the water OH stretching modes vibrate at higher frequencies, while the frequencies of the water and methane bending modes overlap even at low pressure.

Over the pressure range considered here, methane–water frame distances along the trajectories remain longer than the typical ones for strong hydrogen bonds (Supporting Information Figure S8). Also, the orientation of two CH bonds that point toward hollow sites of the water frame rather than oxygen atoms is consistent with mostly repulsive interactions between CH_4 and the water frame. More details on the mode coupling in protonated $\text{CH}_4-(\text{H}_2\text{O})_2$ hydrate can be found in Supporting Information (Figures S8 and S13).

We note that the methane rocking mode, herein measured for the first time to the best of our knowledge (Supporting Information Figure S6), becomes more defined and intense as the pressure increases. This is likely a consequence of the guest orientational ordering.

CONCLUSIONS

To conclude, our study shows that the evolution from an enclathrated almost free rotor to a strongly interacting $\text{CH}_4:\text{D}_2\text{O}$ compound is rather complex and passes through several stages: first, the orientational ordering of the methane molecules in a $A-B$ pairwise fashion in the channels along the c axis; second, the progressive locking-in of A_+/A_- and B_+/B_- methane rotations mainly due to steric hindrance and which is complete from 20 GPa onward, along with methane angular distortion; and third, a strong coupling between the guest and host modes, with deep consequences on the very distinction between the methane and the water DoF.

Therefore, the system undergoes a transformation from a pure hydrophobic hydrated nonstoichiometric material (still with noticeable vdW interactions) to a strongly interacting, probably a stoichiometric mixed molecular crystal. Analyzing in more detail the possibility of H-bonding between the water host and methane guest molecules, we find no hint of such an interaction even at the maximum pressure investigated here. In contrast with what was observed for methane molecules absorbed in hydroxyl-decorated MOF, where a clear $\text{D}_4\text{C}^{\text{guest}} \cdots \text{H}-\text{O}^{\text{host}}$ binding interaction is present,⁴⁸ in methane-filled ice the guest–host mode coupling is rather driven by repulsive interactions even under the tight confinement conditions reached at the high pressure.

ASSOCIATED CONTENT

Supporting Information

The Supporting Information is available free of charge on the ACS Publications website at DOI: 10.1021/acs.jpcc.8b02783.

X-ray diffraction, Raman spectra, fitting procedure, CH_4 rocking mode, lattice parameters, change of compressibility, pair correlation functions, QTB description, and methane stretching mode splitting analysis (PDF)

AUTHOR INFORMATION

Corresponding Authors

*E-mail: fabio.finocchi@sorbonne-universite.fr (F.F.).

*E-mail: livia.bove@sorbonne-universite.fr. Phone: +33 (0) 144275116, +33 (0)144275219 (L.E.B.).

ORCID 

Sofiane Schaack: 0000-0002-6526-9989

Umbertoluca Ranieri: 0000-0003-2026-6132

Andrzej Falenty: 0000-0001-5995-9900

Notes

The authors declare no competing financial interest.

ACKNOWLEDGMENTS

This work was granted access to the HPC resources of CINES under the allocation A0010906719 made by GENCI. The experimental work was supported by the Swiss National Science Fund under grant number 200021_149487. The authors acknowledge influential remarks by Simon Huppert and constructive criticism by our referees.

REFERENCES

- (1) Jeffrey, G. A. Water structure in organic hydrates. *Acc. Chem. Res.* **1969**, *2*, 344–352.
- (2) Sloan, E.; Koh, C. *Clathrate Hydrates of Natural Gases*, 3rd ed.; CRC press: Boca Raton, 2007.
- (3) Hummer, G.; Garde, S.; Garcia, A. E.; Paulaitis, M. E.; Pratt, L. R. The pressure dependence of hydrophobic interactions is consistent with the observed pressure denaturation of proteins. *Proc. Natl. Acad. Sci. U. S. A.* **1998**, *95*, 1552–1555.
- (4) Mao, W. L.; Mao, H.-k. Hydrogen storage in molecular compounds. *Proc. Natl. Acad. Sci. U. S. A.* **2004**, *101*, 708–710.
- (5) Struzhkin, V. V.; Militzer, B.; Mao, W. L.; Mao, H.-k.; Hemley, R. J. Hydrogen storage in molecular clathrates. *Chem. Rev.* **2007**, *107*, 4133–4151.
- (6) Brewer, P. G.; Friederich, G.; Peltzer, E. T.; Orr, F. M. Direct experiments on the ocean disposal of fossil fuel CO₂. *Science* **1999**, *284*, 943–945.
- (7) Demirbas, A. *Green Energy and Technology*; Springer: London, 2010.
- (8) Loveday, J. S.; Nelmes, R. J. High-pressure neutron diffraction and models of Titan. *High Pressure Res.* **2003**, *23*, 41–47.
- (9) Loveday, J. S.; Nelmes, R. J.; Guthrie, M.; Klug, D. D.; Tse, J. S. Transition from cage clathrate to filled ice: The structure of methane hydrate III. *Phys. Rev. Lett.* **2001**, *87*, 215501.
- (10) Loveday, J. S.; Nelmes, R. J. High-pressure gas hydrates. *Phys. Chem. Chem. Phys.* **2008**, *10*, 937–950.
- (11) Hirai, H.; Kondo, T.; Hasegawa, M.; Yagi, T.; Yamamoto, Y.; Komai, T.; Nagashima, K.; Sakashita, M.; Fujihisa, H.; Aoki, K. Methane hydrate behavior under high pressure. *J. Phys. Chem. B* **2000**, *104*, 1429–1433.
- (12) Hirai, H.; Uchihara, Y.; Fujihisa, H.; Sakashita, M.; Katoh, E.; Aoki, K.; Nagashima, K.; Yamamoto, Y.; Yagi, T. High-pressure structures of methane hydrate observed up to 8 GPa at room temperature. *J. Chem. Phys.* **2001**, *115*, 7066–7070.
- (13) Hirai, H.; Tanaka, T.; Kawamura, T.; Yamamoto, Y.; Yagi, T. Retention of filled ice structure of methane hydrate up to 42 GPa. *Phys. Rev. B: Condens. Matter Mater. Phys.* **2003**, *68*, 172102.
- (14) Hirai, H.; Machida, S.-i.; Kawamura, T.; Yamamoto, Y.; Yagi, T. Stabilizing of methane hydrate and transition to a new high-pressure structure at 40 GPa. *Am. Mineral.* **2006**, *91*, 826–830.
- (15) Machida, S.-i.; Hirai, H.; Kawamura, T.; Yamamoto, Y.; Yagi, T. A new high-pressure structure of methane hydrate surviving to 86 GPa and its implications for the interiors of giant icy planets. *Phys. Earth Planet. Inter.* **2006**, *155*, 170–176.
- (16) Chou, I.-M.; Sharma, A.; Burruss, R. C.; Shu, J.; Mao, H.-k.; Hemley, R. J.; Goncharov, A. F.; Stern, L. A.; Kirby, S. H. Transformations in methane hydrates. *Proc. Natl. Acad. Sci. U. S. A.* **2000**, *97*, 13484–13487.
- (17) Kumazaki, T.; Kito, Y.; Sasaki, S.; Kume, T.; Shimizu, H. Single-crystal growth of the high-pressure phase II of methane hydrate and its Raman scattering study. *Chem. Phys. Lett.* **2004**, *388*, 18–22.
- (18) Shimizu, H.; Kumazaki, T.; Kume, T.; Sasaki, S. In situ observations of high-pressure phase transformations in a synthetic methane hydrate. *J. Phys. Chem. B* **2002**, *106*, 30–33.
- (19) Machida, S.-i.; Hirai, H.; Kawamura, T.; Yamamoto, Y.; Yagi, T. Raman spectra of methane hydrate up to 86 GPa. *Phys. Chem. Miner.* **2007**, *34*, 31–35.
- (20) Choukroun, M.; Grasset, O.; Tobie, G.; Sotin, C. Stability of methane clathrate hydrates under pressure: Influence on outgassing processes of methane on Titan. *Icarus* **2010**, *205*, 581–593.
- (21) Tanaka, T.; Hirai, H.; Matsuoka, T.; Ohishi, Y.; Yagi, T.; Ohtake, M.; Yamamoto, Y.; Nakano, S.; Irifune, T. Phase changes of filled ice Ih methane hydrate under low temperature and high pressure. *J. Chem. Phys.* **2013**, *139*, 104701.
- (22) Klug, D. D.; Tse, J. S.; Liu, Z.; Hemley, R. J. Hydrogen-bond dynamics and Fermi resonance in high-pressure methane filled ice. *J. Chem. Phys.* **2006**, *125*, 154509.
- (23) Iitaka, T.; Ebisuzaki, T. Methane hydrate under high pressure. *Phys. Rev. B: Condens. Matter Mater. Phys.* **2003**, *68*, 172105.
- (24) Ranieri, U.; Koza, M. M.; Kuhs, W. F.; Klotz, S.; Falenty, A.; Gillet, P.; Bove, L. E. Fast methane diffusion at the interface of two clathrate structures. *Nat. Commun.* **2017**, *8*, 1076.
- (25) Del Rosso, L.; Celli, M.; Ulivi, L. New porous water ice metastable at atmospheric pressure obtained by emptying a hydrogen-filled ice. *Nat. Commun.* **2016**, *7*, 13394.
- (26) Amos, D. M.; Donnelly, M.-E.; Teeratchanan, P.; Bull, C. L.; Falenty, A.; Kuhs, W. F.; Hermann, A.; Loveday, J. S. A Chiral Gas–Hydrate Structure Common to the Carbon Dioxide–Water and Hydrogen–Water Systems. *J. Phys. Chem. Lett.* **2017**, *8*, 4295–4299.
- (27) Baumert, J.; Gutt, C.; Shpakov, V. P.; Tse, J. S.; Krisch, M.; Müller, M.; Requardt, H.; Klug, D. D.; Janssen, S.; Press, W. Lattice dynamics of methane and xenon hydrate: Observation of symmetry-avoided crossing by experiment and theory. *Phys. Rev. B: Condens. Matter Mater. Phys.* **2003**, *68*, 174301.
- (28) Schober, H.; Itoh, H.; Klapproth, A.; Chihai, V.; Kuhs, W. F. Guest-host coupling and anharmonicity in clathrate hydrates. *Eur. Phys. J. E* **2003**, *12*, 41–49.
- (29) Bezacier, L.; Le Menn, E.; Grasset, O.; Bollengier, O.; Oancea, A.; Mezouar, M.; Tobie, G. Experimental investigation of methane hydrates dissociation up to 5 GPa: Implications for Titan's interior. *Phys. Earth Planet. Inter.* **2014**, *229*, 144–152.
- (30) Loveday, J. S. *High-Pressure Crystallography*; Katrusiak, A., McMillan, P., Eds.; Springer: Netherlands, Dordrecht, 2004; pp 69–80.
- (31) Giannozzi, P.; Baroni, S.; Bonini, N.; Calandra, M.; Car, R.; Cavazzoni, C.; Ceresoli, D.; Chiarotti, G. L.; Cococcioni, M.; Dabo, I.; et al. QUANTUM ESPRESSO: A modular and open-source software project for quantum simulations of materials. *J. Phys.: Condens. Matter* **2009**, *21*, 395502.
- (32) Dammak, H.; Chalopin, Y.; Laroche, M.; Hayoun, M.; Greffet, J.-J. Quantum thermal bath for molecular dynamics simulation. *Phys. Rev. Lett.* **2009**, *103*, 190601.
- (33) Bronstein, Y.; Depondt, P.; Finocchi, F.; Saitta, A. M. Quantum-driven phase transition in ice described via an efficient Langevin approach. *Phys. Rev. B: Condens. Matter Mater. Phys.* **2014**, *89*, 214101.
- (34) Bronstein, Y.; Depondt, P.; Bove, L. E.; Gaal, R.; Saitta, A. M.; Finocchi, F. Quantum versus classical protons in pure and salty ice under pressure. *Phys. Rev. B: Condens. Matter Mater. Phys.* **2016**, *93*, 024104.
- (35) Briec, F.; Bronstein, Y.; Dammak, H.; Depondt, P.; Finocchi, F.; Hayoun, M. Zero-point energy leakage in quantum thermal bath molecular dynamics simulations. *J. Chem. Theory Comput.* **2016**, *12*, 5688–5697.
- (36) Ceriotti, M.; Manolopoulos, D. E.; Parrinello, M. Accelerating the convergence of path integral dynamics with a generalized Langevin equation. *J. Chem. Phys.* **2011**, *134*, 084104.
- (37) Kuhs, W. F.; Staykova, D. K.; Salamatina, A. N. Formation of methane hydrate from polydisperse ice powders. *J. Phys. Chem. B* **2006**, *110*, 13283–13295.

- (38) Datchi, F.; Dewaele, A.; Le Godec, Y.; Loubeyre, P. Equation of state of cubic boron nitride at high pressures and temperatures. *Phys. Rev. B: Condens. Matter Mater. Phys.* **2007**, *75*, 214104.
- (39) Dewaele, A.; Torrent, M.; Loubeyre, P.; Mezouar, M. Compression curves of transition metals in the Mbar range: Experiments and projector augmented-wave calculations. *Phys. Rev. B: Condens. Matter Mater. Phys.* **2008**, *78*, 104102.
- (40) Bove, L. E.; Gaal, R.; Raza, Z.; Ludl, A.-A.; Klotz, S.; Saitta, A. M.; Goncharov, A. F.; Gillet, P. Effect of salt on the H-bond symmetrization in ice. *Proc. Natl. Acad. Sci. U. S. A.* **2015**, *112*, 8216–8220.
- (41) Calvo, F.; Van-Oanh, N.-T.; Parneix, P.; Falvo, C. Vibrational spectra of polyatomic molecules assisted by quantum thermal baths. *Phys. Chem. Chem. Phys.* **2012**, *14*, 10503–10506.
- (42) Perdew, J. P.; Burke, K.; Ernzerhof, M. Generalized gradient approximation made simple. *Phys. Rev. Lett.* **1996**, *77*, 3865.
- (43) Grimme, S. Semiempirical GGA-type density functional constructed with a long-range dispersion correction. *J. Comput. Chem.* **2006**, *27*, 1787–1799.
- (44) Ceriotti, M.; More, J.; Manolopoulos, D. E. i-PI: A Python interface for ab initio path integral molecular dynamics simulations. *Comput. Phys. Commun.* **2014**, *185*, 1019.
- (45) Hiratsuka, M.; Ohmura, R.; Sum, A. K.; Yasuoka, K. Vibrational modes of methane in the structure H clathrate hydrate from ab initio molecular dynamics simulation. *J. Chem. Phys.* **2012**, *137*, 144306.
- (46) Chen, P.-N.; Zha, C.-S.; Chen, X.-J.; Shu, J.; Hemley, R. J.; Mao, H.-k. Raman study of phase transitions in compressed methane using moissanite anvil cells. *Phys. Rev. B: Condens. Matter Mater. Phys.* **2011**, *84*, 104110.
- (47) Bini, R.; Pratesi, G. High-pressure infrared study of solid methane: Phase diagram up to 30 GPa. *Phys. Rev. B: Condens. Matter Mater. Phys.* **1997**, *55*, 14800.
- (48) Savage, M.; Da Silva, I.; Johnson, M.; Carter, J. H.; Newby, R.; Suyetin, M.; Besley, E.; Manuel, P.; Rudić, S.; Fitch, A. N.; et al. Observation of binding and rotation of methane and hydrogen within a functional metal–organic framework. *J. Am. Chem. Soc.* **2016**, *138*, 9119–9127.